AIAA 2002-1745

INTRALAMINAR AND INTERLAMINAR PROGRESSIVE FAILURE ANALYSES OF COMPOSITE PANELS WITH CIRCULAR CUTOUTS

Vinay K. Goyal*
Virginia Polytechnic Institute and State University, Blacksburg, VA 24061-0203
Navin Jaunky†
Institute for Computer Applications in Science and Engineering, Hampton, VA, 23681
Eric R. Johnson‡
Virginia Polytechnic Institute and State University, Blacksburg, VA 24061-0203
Damodar Ambur§
NASA Langley Research Center, Hampton, VA, 23681

Abstract

A progressive failure methodology is developed and demonstrated to simulate the initiation and material degradation of a laminated panel due to intralaminar and interlaminar failures. Initiation of intralaminar failure can be by a matrix-cracking mode, a fiber-matrix shear mode, and a fiber failure mode. Subsequent material degradation is modeled using damage parameters for each mode to selectively reduce lamina material properties. The interlaminar failure mechanism such as delamination is simulated by positioning interface elements between adjacent sublaminates. A nonlinear constitutive law is postulated for the interface element that accounts for a multi-axial stress criteria to detect the initiation of delamination, a mixed-mode fracture criteria for delamination progression, and a damage parameter to prevent restoration of a previous cohesive state. The methodology is validated using experimental data available in the literature on the response and failure of quasi-isotropic panels with centrally located circular cutouts loaded into the postbuckling regime. Very good agreement between the progressive failure analyses and the experimental results is achieved if the failure analyses includes the interaction of intralaminar and interlaminar failures.

Introduction

The phenomenon of delamination in laminated composite structures usually originates from discontinuities such as matrix cracks, or the presence of free edges. Delamination may lead to reduced stiffness and strength. In some cases delamination can provide stress relief and delay final failure of the structure. The ability to accurately predict damage evolution is essential for predicting the performance of composite structures and developing reliable and safe designs. In recent years, progressive failure analyses (PFA) in composite laminates has been the focus of extensive research. In most of the PFA either intralaminar or delamination damage mechanism are considered.

In past studies when fracture mechanics based approaches are used, an initial delaminated area and self-similar delamination growth and is often assumed[1,2]. These limitations can be overcome by positioning interface elements between adjacent laminae of a composite structure. With this methodology, the prediction of initiation and progression of delamination without specifying an initial delaminated area becomes natural without imposing constraints in the PFA. Moreover, with interface elements, the prediction of non-self similar delamination growth is possible. Interface elements can be used in a variety of problems involving buckling and in the presence of a delamination. Shahwan and Waas[3] investigated the interaction of buckling and delamination of a panel with a circular hole subjected to compressive loads. A mixed-mode damage model was developed by de Moura et al.[4] to simulate delamination growth in a compression panel after it was subjected to a low velocity impact event. They showed that the internal delaminations reduced the compressive strength of the laminate. The interaction of delamination with buckling phenomena in a simple structural problem is discussed by Allix and Corigliano[5].

Intralaminar failure can initiate and interact with, delamination and visa versa which could lead to more significant and adverse changes in response characteristics of the structure. Therefore, the study of this interaction is important. Few researchers have considered both, intralaminar damage and delamination in the PFA. Daudeville et al.[6] studied the progression of delamination near the hole of a perforated plate under tensile loads. Geubelle and Baylor[7] simulated complex failure mechanisms such as matrix cracking and delamination that occur when thin composite plates are subjected to low-velocity impact. Dávila et al.[8] analyzed the debonding

*Graduate Research Assistant, Aerospace and Ocean Engineering Department. Student Member, AIAA.
†Senior Staff Scientist. Member, AIAA.
‡Professor, Aerospace and Ocean Engineering Department. Senior Member AIAA and Member ASME
§Head, Mechanics and Durability Branch. Associate Fellow, AIAA.

Copyright © 2002 by Vinay K. Goyal Published by the American Institute of Aeronautics and Astronautics, Inc. with permission.

of skin-stringer constructions using a step-by-step simulation of material degradation based on strain softening decohesion elements and a ply degradation procedure.

To the authors' knowledge, in the literature concerning PFA, no work was reported that studied the interaction of the shell buckling and postbucking response with intralaminar and interlaminar damage mechanisms. The objective of this paper is to assess a developed progressive failure methodology by simulating the geometrically nonlinear response and failure of a flat panel tested in shear[9] and a curved panel tested in axial compression.[10] Both of these test panels contained a centrally located circular cutout that acts as a stress raiser and, consequently, a site for failure initiation. The paper is structured with descriptions of (i) progressive failure methodology, (ii) interlaminar PFA, (iii) intralaminar PFA, (iv) numerical simulations of the flat panel and curved panels, and (vii) concluding remarks.

Progressive Failure Methodology

A progressive failure methodology is developed that is an extension of the methodologies found in Pifko and Kushner[11] and Sleight et al.[12] The methodology requires a nonlinear solver to establish equilibrium because both geometric and material nonlinearity are considered. The geometric nonlinearity is due to large strain and large rotation kinematics. The nonlinear material behavior is due to the degradation of the material properties of the plies and the material in between the plies to simulate intralaminar and interlaminar damage mechanisms. An incremental-iterative approach is adopted for the nonlinear finite element analysis, and the Newton-Raphson method is used to trace the loading path of the structure with a displacement-control analysis. A line search algorithm is only activated to provide an initial approximation to the Newton-Raphson method, or to minimize a large residual force.

The progressive failure methodology complies with two requirements[13]: (i) appropriate load steps to achieve solution convergence while representing accurately local load redistribution, and (ii) a fine mesh in regions that undergo material degradation to represent proper stress gradients at the boundary of the damaged zones. A typical methodology for PFA that includes both intralaminar and interlaminar failures is illustrated in Figure 1. The methodology is similar to the one used by Dávila et al.[8] Under displacement control, let w_i denote the applied displacement at the i displacement step. Assume equilibrium was established at the $(i-1)$ displacement step, and assume a small increment in the displacement $\triangle w$ such that $w_i = w_{i-1} + \triangle w$. The objective is to obtain the equilibrium state at w_i, which is equivalent to obtaining the corresponding reaction force P_i. At each iteration in the Newton-Raphson method, we check for intralaminar and interlaminar failures. If the intralaminar failure is detected, then the material properties of the affected plies are degraded. If the interlaminar failure is detected, then the delamination is initiated or advanced by degrading interlaminar material properties. If any failure is detected during this iteration, an additional iteration may be needed to obtain a converged solution. When a converged solution is obtained, the reaction force P_i associated to the applied displacement w_i is computed, and the material state is saved. Then the whole procedure is repeated with the next displacement step w_{i+1}. In the event that the maximum number of iterations to obtain a converged solution is exceeded, the displacement step w_i is repeated with a smaller increment $\triangle w$. The PFA is stopped when the procedure cannot be repeated with a smaller increment because the increment is already too small with respect to a number close to 10^{-10}. The structural response is characterized by (w_i, P_i).

The above methodology is implemented in the structural analysis code ABAQUS[14]. The next two sections discuss further details on the interlaminar PFA and intralaminar PFA.

Interlaminar Damage

Interface elements are positioned between composite laminae in potential delamination sites to predict initiation and progression of delamination. The softening constitutive law developed in Goyal et al.[15] is adopted in this paper for the formulation of the interface element. The constitutive law mathematically describes the initiation of delamination, the evolution of the degradation zone, and delamination growth. The initiation and progression of delamination occurs when an effective maximum interfacial strength and the local surface fracture energy is, respectively, exceeded.

An interface element consists of an upper surface S^+ and a lower surface S^- initially coincident and connected by a continuous distribution of nonlinear springs as shown in Figure 2a. The points P^+ and P^- are also initially coincident and contained in S^+ and S^-, respectively. The relative displacements between these points across the interface are related to the cohesive tractions that act to resist Mode I opening or the Mode II and Mode III sliding of the upper and lower surface. The resistive tractions that are associated to the relative displacements at a point A are shown in Figure 2a. The interlaminar normal traction is denoted T_3 and the tangential tractions are denoted T_1 and T_2. The maximum interfacial strengths are $T_j^c, j = 1, 2, 3$. The relative displacement in the j-th direction is $\triangle_j$ and its respective critical separation value is $\triangle_j^c$. For simplicity, $\triangle_j$ and T_j are normalized with respect to $\triangle_j^c$ and T_j^c, respectively as follows: $\bar{\triangle}_j = \triangle_j / \triangle_j^c$, and $\bar{T}_j = T_j / T_j^c$ for $j = 1, 2, 3$. A mixed-mode scalar parameter μ given by

$$\mu = \left(\left|\bar{\triangle}_1\right|^\alpha + \left|\bar{\triangle}_2\right|^\alpha + \langle \bar{\triangle}_3 \rangle^\alpha \right)^{1/\alpha} \tag{1}$$

couples the sliding displacements to the opening displacement, where α is a material parameter. Here, $|x|$ denotes the absolute value of x, and $\langle x \rangle$ is x for $x > 0$, otherwise it is zero. The softening constitutive law is expressed as

$$\begin{Bmatrix} \bar{T}_1 \\ \bar{T}_2 \\ \bar{T}_3 \end{Bmatrix} = \begin{Bmatrix} \bar{\triangle}_1 \\ \bar{\triangle}_2 \\ \langle \bar{\triangle}_3 \rangle \end{Bmatrix} \exp\left(\frac{2 - \mu^\beta / \tilde{d} - \tilde{d}}{\beta} \right) + \begin{Bmatrix} 0 \\ 0 \\ \langle -\bar{\triangle}_3 \rangle \end{Bmatrix} \exp(1 - \kappa \bar{\triangle}_3) \tag{2}$$

The parameter κ, $\kappa \geq 1$, is an interpenetration factor to magnify the repulsive force T_3 to avoid interpenetration of the upper and lower surfaces of the interface element. The parameter β defines the length of the softening zone, and $\tilde{d}$ is an internal state variable to prevent the restoration of the previous cohesive state, given by

$$\tilde{d}^{(i)} = \max\left(1, \tilde{d}^{(i-1)}, \mu_{(i)}^{\beta}\right), \quad \tilde{d}^{(0)} = 1 \tag{3}$$

where i is the displacement step. The constitutive law satisfies a multi-axial stress criterion for delamination initiation and a mixed-mode fracture criterion for delamination progression,

$$T_e = \left(\left(\frac{T_1}{T_1^c}\right)^{\alpha} + \left(\frac{T_2}{T_2^c}\right)^{\alpha} + \left(\frac{\langle T_3\rangle}{T_3^c}\right)^{\alpha}\right)^{1/\alpha} = 1 \tag{4}$$

$$\left(\frac{G_I}{G_{Ic}}\right)^{\alpha/2} + \left(\frac{G_{II}}{G_{IIc}}\right)^{\alpha/2} + \left(\frac{G_{III}}{G_{IIIc}}\right)^{\alpha/2} = 1 \tag{5}$$

and α is a material parameter that determines the shape of the failure surface. The empirical parameters in the constitutive law are the critical energy release rates G_{Ic}, G_{IIc}, G_{IIIc}; the maximum interfacial strengths T_1^c, T_2^c, T_3^c; and the parameter β. These parameters can be specified so that the critical separation values $\triangle_j^c, j = 1, 2, 3$ are obtained from

$$G_{Ic} = \int_0^{\infty} T_3(0, 0, \triangle_3) d\triangle_3 = T_3^c \, \triangle_3^c \, \eta \tag{6}$$

$$G_{IIc} = \int_0^{\infty} T_1(\triangle_1, 0, 0) d\triangle_1 = T_1^c \, \triangle_1^c \, \eta$$

$$G_{IIIc} = \int_0^{\infty} T_2(0, \triangle_2, 0) d\triangle_2 = T_2^c \, \triangle_2^c \, \eta$$

$$\eta = \beta^{(2-\beta)/\beta} \, \Gamma\left[\frac{2}{\beta}\right] \exp\left(\frac{1}{\beta}\right)$$

where $\Gamma[z]$ is the gamma Euler function of z.

In Figure 2b, the effective traction T_e defined in Equation 4 is plotted versus the effective scalar parameter μ for $\beta = 1$ and independent of α. The form of the constitutive law is such that with increasing μ the effective traction T_e attains a maximum, decreases, and eventually vanishes. If unloading occurs at $\mu = 2$, the accumulated damage is $\tilde{d} = 2$, and the path denoted as 'C' is followed. Upon reloading, path 'C' is retraced followed by path 'D'.

The finite element formulation is based on the principle of virtual work and is developed in the paper by Goyal et al.[15] The 3×3 material tangent stiffness matrix $\mathbf{D}$ is required for the computation of the tangent stiffness matrix. The expressions are given in Goyal et al.[15] For the numerical simulations, the following modification to $\mathbf{D}$ avoids numerical convergence difficulties in the nonlinear solution procedure[15]

$$D_{ii} = \max(0, D_{ii}) \tag{7}$$

It is assumed that $\kappa = 1$, $\alpha = 2$, and $\beta = 2$. The eight node isoparametric interface element for three-dimensional analysis shown in Figure 2c was implemented in the commercial finite element code ABAQUS as an UEL subroutine[14].

Intralaminar Damage

The failure criteria applied in the present analysis are those for unidirectional fiber composite materials as proposed by Hashin[16] with slight modifications to the elastic stiffness degradation models developed for compression by Chang and Lessard.[17] The intralaminar failure modes considered in these references are matrix-cracking, fiber-matrix shear failure, and fiber failure.

The stresses are computed in the principal directions for each ply orientation and used in the unidirectional failure criteria. The failure criteria are in terms of the stresses σ, the shear allowables S, and the strengths X and Y. The in-plane stresses are σ_{11}, σ_{22}, and τ_{12}, and the transverse shear stresses are τ_{13}, and τ_{23}. The in-plane shear strength is S_{12}, and the transverse shear strengths are S_{13}, and S_{23}. The strength perpendicular and parallel to the fiber direction is denoted as Y and X, respectively. The subscripts 'c' and 't' denote compression and tension, respectively.

Fiber failure occurs due to tension or compression independent of the other stress components. In compression the fiber fails by buckling. The failure index e_f is

$$e_f^2 = \left(\frac{\sigma_{11}}{X_c}\right)^2, \quad \sigma_{11} < 0 \tag{8}$$

$$e_f^2 = \left(\frac{\sigma_{11}}{X_t}\right)^2, \quad \sigma_{11} > 0$$

The failure index e_m for matrix cracking is,

$$e_m^2 = \frac{\sigma_{22}}{Y_c}\left[\left(\frac{Y_c}{2S_{23}}\right)^2 - 1\right] + \left(\frac{\sigma_{22}}{2S_{23}}\right)^2 + \left(\frac{\tau_{12}}{S_{12}}\right)^2 + \left(\frac{\tau_{13}}{S_{13}}\right)^2 + \left(\frac{\tau_{23}}{S_{23}}\right)^2, \quad \sigma_{22} < 0 \tag{9}$$

$$e_m^2 = \left(\frac{\sigma_{22}}{Y_t}\right)^2 + \left(\frac{\tau_{12}}{S_{12}}\right)^2 + \left(\frac{\tau_{13}}{S_{13}}\right)^2 + \left(\frac{\tau_{23}}{S_{23}}\right)^2, \quad \sigma_{22} > 0$$

Fiber-matrix shear failure occurs due to a combination of axial stress σ_{11} and the shear stresses. The failure index e_s is

$$e_s^2 = \left(\frac{\langle -\sigma_{11}\rangle}{X_c}\right)^2 + \left(\frac{\tau_{12}}{S_{12}}\right)^2 + \left(\frac{\tau_{13}}{S_{13}}\right)^2 \tag{10}$$

where $\langle -\sigma_{11}\rangle = 0$, for $\sigma_{11} > 0$ and $\langle \sigma_{11}\rangle = \sigma_{11}$ otherwise.

To simulate the failure modes, the elastic properties are made linearly dependent on internal state variables d_m, d_f, and d_s. These variables are bounded by $0 \leq d_m, d_f, d_s \leq 1$, with $d = 0$ undamaged and $d = 1$ representing fully damaged states, respectively. The relation between the internal state variables and the failure indices is,

$$d_j = \min\left(1, \frac{\langle e_j^2 - \epsilon\rangle}{1 - \epsilon}\right) \tag{11}$$

with $j = m, f, s$. The parameter ϵ is a small number and is close to 1. The internal state variables are made history

dependent to prevent restoration of the previous failure state with

$$d_j^{(i)} = \max\left(d_j^{(i-1)}, 0\right), \quad d_j^{(0)} = 0 \tag{12}$$

where i is the displacement step and $j = m, f, s$.

The degraded material properties $\mathbf{w}'$ are related to the undamaged material properties $\mathbf{w}$ through a damage operator. The undamaged and degraded material properties in vector form are

$$\begin{aligned} \mathbf{w} &= \{E_{11}, E_{22}, \nu_{12}, G_{12}, G_{13}, G_{23}\}^{\mathrm{T}} \\ \mathbf{w}' &= \{E'_{11}, E'_{22}, \nu'_{12}, G'_{12}, G'_{13}, G'_{23}\}^{\mathrm{T}} \end{aligned} \tag{13}$$

The damage operator $\mathbf{F}$ is a diagonal matrix given by

$$\begin{aligned} f_{11} &= \varphi_1 \max(0, d_f) \\ f_{22} &= \varphi_2 \max(0, d_m, d_f) \\ f_{33} &= \varphi_3 \max(0, d_m, d_s, d_f) \\ f_{44} &= \varphi_4 \max(0, d_s, d_f) \\ f_{55} &= \varphi_5 \max(0, d_s, d_f) \\ f_{66} &= \varphi_6 \max(0, d_f) \end{aligned} \tag{14}$$

and $\varphi_j, \varphi_j \leq 1, j = 1, ..., 6$ is the fraction of reduction of the material properties. Ill-conditioned matrices often arise if $\varphi = 1$. The degradation scheme is applied with

$$\mathbf{w}' = (\mathbf{I} - \mathbf{F})\mathbf{w} \tag{15}$$

and $\mathbf{I}$ is the 6×6 identity matrix. Fiber failure affects all of the material properties, matrix cracking affects the material properties E_{22} and ν_{12}, and fiber-matrix shear affects three material properties ν_{12}, G_{12}, and G_{13}.

The finite element implementation of the failure analysis presented here was developed for the ABAQUS structural analysis software using the user subroutine USDFLD[14]. The USDFLD invokes the material properties and the stresses of all the integration points of the elements. At each integration point, the failure criteria are evaluated and the damage operator $\mathbf{F}$ is applied to the material properties.

Numerical Simulations

Finite element models were developed for a flat composite panel subjected to in-plane shear and a curved panel subjected to axial compression. Both panels contain centrally located circular cutouts, and both are made from AS4-3502 graphite-epoxy pre-impregnated tape material. Quasi-static test results for the shear panel and the curved panel are given by Rouse[9] and Hilburger et al.[10], respectively. Finite element models of these test specimens are shown in Figure 3a and Figure 3b. Material moduli used in the analyses are listed in Table 1, the intralaminar strength allowables in Table 2, and the critical energy release rates and maximum interfacial strengths used in the analyses are listed in Table 3.

The test section of the shear panel shown in Figure 3a is a 12-inch square, and the diameter of the cutout is 1.0 in. The laminate has 24 plies with a stacking sequence of $[\pm 45/0_2]_{3s}$ and a nominal ply thickness of 0.0055 in. The

Table 1 Mechanical Properties for Graphite-Epoxy

E_{11}	E_{22}	G_{12}, G_{13}	G_{23}	ν_{12}
18.5 Msi	1.67 Msi	0.87 Msi	0.258 Msi	0.25

Table 2 Intralaminar Strength Allowables for Graphite-Epoxy

X_t	X_c	Y_t	Y_c	S_{12}	S_{13}, S_{23}
200.0 ksi	180.0 ksi	12.6 ksi	24.6 ksi	25.5 ksi	4.8 ksi

Table 3 Interface Material Properties for Graphite-Epoxy

T_2^c, T_3^c	T_1^c	G_{Ic}	G_{IIc}, G_{IIIc}
10.5 ksi	9.0 ksi	1.31 lb/in.	3.30 lb/in.

picture frame fixture is made of steel plates 2.75-in. wide and 6.75-in. thick. The steel plates were modeled using ABAQUS four node, shear deformable S4 elements that were restrained in the out-of-plane direction. The test section was modeled using ABAQUS four node shear deformable S4R elements. Element S4R has four nodes with six degrees of freedom per node, it is transverse shear deformable, and reduced integration is used to compute its stiffnesses. Three integration points through each ply thickness are used in the analysis. The pin joints at the four corners of the fixture are enforced by using multiple-point constraints. The 1- and 2-direction displacements of the loading pin are specified to be of the same value so that the resultant displacement w is along the diagonal. The in-plane displacements of the pin joint diagonally opposite to the loading pin are specified to be zero. An initial geometric imperfection of the panel was included in the analysis. This imperfection is in the shape of the equilibrium state of the panel subjected to a pressure acting normal to the panel, which is scaled so that the maximum amplitude of the shape is 1% of the laminate thickness. This shape is similar to one half-wave in the 1-2 directions of the panel.

The curved panel geometry and boundary conditions and loading are shown in Figure 3b. The radius R of the cylindrical panel is 15-in., its length $L = 14.75$ in., and its width $W = 14.5$ in. Two curved panels were analyzed. One panel had cutout diameter-to-width ratio $d/W = 0.2$ with a measured ply thickness of 0.00529 in., the other had $d/W = 0.4$ with a measured ply thickness of 0.00542 in. Both panels have a laminate stacking sequence of $[\pm 45/0/90]_{3s}$. A uniform, compressive axial displacement w was specified along the curved edge, while the axial displacement on the opposite edge is specified to be zero. The curved panel was modeled using ABAQUS four node shear deformable S4R elements.

Visual analysis from the failed test specimens show that delamination mostly occurred at the midplane of the flat panel loaded in shear and the curved panel with $d/W = 0.4$ loaded

in compression. For the curved panel with $d/W = 0.2$, delamination occurred in multiple locations throughout the thickness. Positioning interface elements between every pair of adjacent laminae is computationally expensive. Therefore, as an approximation to the analysis, interface elements are used to model delamination at the midplane of the laminate in the vicinity of the cutout. The interface element is depicted in Figure 2c, and it is an eight node, isoparametric element, with three translational degrees of freedom per node. The nodes of the interface elements were made coincidental with those of the top and bottom sublaminates by moving the sublaminate reference surfaces to coincide with the midplane of the shell wall. A typical finite element model of a panel consists of approximately 7,000 nodes and 10,000 elements with 38,000 degrees of freedom, and required about 173,000 CPU seconds to execute on a SUN 450. The size of a typical element near the edge of the cutout was 0.07 inches square.

Results of the flat panel loaded in shear

For the panel, the numerical results from the present analysis and the numerical results from the PFA excluding delamination[18] are compared in Figure 4a with the experimental results reported by Rouse[9]. The load-displacement response is shown in Figure 4a, and the load-strain response is shown in Figure 4b. The strains in the latter figure were measured in the test from back-to-back strain gages bonded to the top and bottom surfaces of the panel, oriented parallel to the loading axis, and located 0.5-in. below the edge of the cutout. These strains correspond to the strain ϵ_{22} measured normal to the fibers in the 45-degree surface plies. The present PFA that includes both intralaminar and interlaminar damage modes is in better agreement with the experimental data than when interlaminar damage mode is not included in the PFA. The buckling load from the test was 25.1 kips and the present analysis prediction is 23.2 kips.

The first material failure was predicted in the postbuckling response. This first failure was a matrix cracking mode occurring at an applied displacement $w = 0.0578$ in. with the corresponding reaction force $P = 27.0$ kips. The location of failure initiation was at the edge of the cutout perpendicular to the load axis. Fringe plots of the intralaminar damage modes in the 0° ply at the midplane in the vicinity of the cutout are shown in Figure 5. The white fringes correspond to damage. At $(w, P) = (0.0590, 28.2)$, the matrix cracking mode occurs at the edge of the cutout perpendicular and parallel to the loading axis as shown in Figure 5a. At $(w, P) = (0.111, 37.6)$, the intralaminar damage modes such as matrix cracking and fiber-matrix shear failure have progressed from the edge of the cutout to the location shown in Figure 5b and 5c.

There are issues in using the post-processor of ABAQUS for the user defined elements. Therefore, contour plots of the von Mises effective stress over the midplane are used to identify regions undergoing delamination growth, since stress concentrations occur ahead of an advancing crack tip. However, these stress contours do not provide information about the shape of the delamination front, but rather they provide information about the direction of delamination growth. Effective stress contours determined from the integration points in the 0° ply closest to the mid-surface and near the edge of the cutout are shown at different applied displacements in Figures 6-7. Initiation of delamination at $(w, P) = (0.073, 32.2)$ is suggested from the von Mises contours plotted in Figure 6a. As shown in Figure 4a the panel collapses at $w = 0.107$ in. At $(w, P) = (0.107, 43.5)$, the delamination progressed approximately one inch from the edge of the cutout in a direction perpendicular to the loading axis, while another delamination initiated at the edge of the cutout along the loading axis, as suggested from Figure 6b. This is confirmed from the deformed plot of the top and bottom sublaminate reference surfaces superimposed on the same plane shown in Figure 7a. These superimposed plots indicate that the shape of the delamination front and suggest that delamination growth is not self-similar. The stress contour plot at $(w, P) = (0.111, 40.0)$ shown in Figure 7b suggests that delamination has progressed approximately 0.75 in. and 1.25 in. from the edge of the cutout along and perpendicular to the loading axis, respectively. The stress contour plot in Figure 7c suggests that delamination has progressed approximately 2.75 in. from the edge of the cutout perpendicular to the loading axis. The arrest of delamination at $(w, P) = (0.112, 30.8)$ along the loading axis is suggested from the stress contours shown in Figure 7c. In this figure, regions of low von Mises stresses extend to a distance of approximately 2 in. from the edge of the cutout along the loading axis. As the panel collapses, the von Mises stresses in these regions along the loading axis are significantly reduced, while rapid delamination growth occurs at approximately 2.75 in. from the edge of the cutout perpendicular to the loading axis. Delamination arrest parallel to the loading axis was later confirmed with a plot of the reference surfaces in the deformed state. To examine the interaction of the intralaminar failure and interlaminar failure, a PFA excluding intralaminar failure was performed. For this case, the PFA predicted delamination initiation at $w = 0.116$ in., whereas the experimental results show that at this applied displacement the panel would have collapsed. Therefore, it was concluded that intralaminar failure mode triggered the initiation of delamination. PFA without the intralaminar failures and PFA without the interlaminar failure were not able to capture the abrupt collapse of the panel. Including both intralaminar and interlaminar failures in the PFA resulted in improved correlation of the analysis and the test results. From the failed specimen it was observed that delamination occurred between plies close to the midplane of the laminate. Therefore, for this structural configuration, interface elements positioned at the midplane of the laminate produced excellent results when compared with the experimental results. In summary, the substantial destabilizing force acting along the compression diagonal caused the panel to buckle. Under continued loading in the postbuckling regime, intralaminar failures initiated and propagated, followed by delaminations initiating at the edge of the cutout in directions perpendicular and parallel to the loading axis. The growth and arrest of these delaminations occur in a complicated manner, with the

collapse of the panel associated with the rapid growth of the delaminations perpendicular to the loading axis.

Results of the curved panels loaded in compression

The load-end shortening responses of the compression loaded curved panels with $d/W = 0.4$ and $d/W = 0.2$ are shown in Figure 8. The numerical results for the panels were compared to the numerical results of the PFA excluding delamination[19] and to the experimental results reported by Hilburger et al.[10] For the panel with $d/W = 0.4$, the present PFA results compare very well with the experimental data.[10] In the analysis where interlaminar damage mode was excluded[19], the response agrees with the experimental results for most part of the loading range. The first failure in the $d/W = 0.4$ panel, as predicted by the present analysis, is a fiber-matrix shear mode at $(w, P) = (0.0382, 21.5)$, which occurs in the midsurface 90°-ply at the edges of the cutout in direction perpendicular to the compressive loading axis. This intralaminar failure occurs before the panel buckles.

Delamination is predicted to initiate at $(w, P) = (0.0530, 26.5)$ at the same location where the intralaminar failure occurred earlier. The initiation of this delamination is suggested by a contour plot of the von Mises stresses shown in Figure 9a, and by a plot of the deformed reference surfaces in Figure 9b of the region labeled as 'A' in Figure 9a. Subsequent to the initiation of delamination, buckling occurred at 27.0 kips compared to the experimental buckling load of 27.2 kips. The analysis by Jaunky et al.[19] predicted buckling at 26.5 kips. As the intralaminar damage progresses from the edge of the cutout in a direction perpendicular to the compressive loading axis, delamination follows in the wake of this degraded material. The direction of progression of delamination and the shape of the delamination front is shown in Figures 10-11 at $(w, P) = (0.0641, 24.7)$. The predicted location of the delamination in the region near the edge of the cutout denoted in Figure 10a as 'B', is the same as the location of the delamination in the failed test specimen shown in Figure 10b. A deformed plot of the reference surfaces of the top and bottom sublaminates is shown in Figure 11a for region 'A' of the cutout. As delamination progresses from the edge of the cutout, crack faces close at the edge of the cutout in its wake. The intensity of the von Mises stresses decrease, indicating that the delamination may have arrested. A plot of the stress contours at a later solution step in the response indicates that delamination no longer grows in region 'A' of the cutout, but the delamination in region 'B' continues to grow. The delamination shape in the region 'B' of the cutout can be seen from the deformation plot of the reference surfaces in Figure 11b. As shown in Figure 8a, the panel continues to carry load at an applied displacement $w = 0.065$ in. A deformed plot of the reference surfaces near the bottom edge of the cutout is shown in Figure 12a at $(w, P) = (0.071, 22.6)$. A comparison of Figure 11b with 12a demonstrates crack faces have closed and delamination is arrested. These results may explain the continued load carrying ability of the panel. The contour plot of the von Mises stresses at panel failure, $(w, P) = (0.076, 22.2)$, is shown in Figure 12b. High stress concentrations at the bottom edge far from the cutout, indicate rapid progression of delamination as the panel fails. In the experiment for the curved panel with $d/W = 0.4$, delamination mostly occurred between plies close to the midplane of the laminate. The present results are in excellent agreement with the experimental data because the interface elements were placed at the midplane of the laminate.

In the experiment for the curved panel with $d/W = 0.2$, buckling resulted in catastrophic failure of the panel, and thus there was no postbuckling strength. From the observations of the failed test specimen, it appeared that delamination may have occurred at multiple sites throughout the thickness. Hence, two analyses were performed. In the first analysis, interface elements were positioned at the midsurface of the laminate. In the second analysis, interface elements were positioned between the bottom $45°/-45°$ laminae. As shown in Figure 8b, the maximum load predicted by the present analyses and the analysis by Jaunky et al.[19] are in good agreement with the experimental value[10]. However, for the present analyses, the collapse of the panel was predicted to occur at a larger applied displacement than the experiment. PFA without interlaminar failure[19] predicts that the panel will carry load after the maximum load is attained, which not is not supported by the experimental results.

For the curved panel with $d/W = 0.2$, matrix cracking, fiber-matrix shear failure, and fiber failure initiated at $(w, P) = (0.0414, 32.5)$. Shortly after the intralaminar failure, delamination initiated at $(w, P) = (0.044, 34.1)$. The deformed plot of the sublaminate reference surfaces near the top and bottom edge of the cutout is shown in Figure 13a and 13b at $(w, P) = (0.0595, 35.7)$ after delamination has progressed in a direction perpendicular to the compressive loading axis. This figure demonstrates the shape of the delamination front. The delamination front has progressed 3.75 in. from the bottom edge of the cutout at the bottom, and at the top edge of the cutout delamination has only progressed 3.0 in. Contour plot of the von Mises stresses near the edge of the cutout is depicted in Figure 13c. At this applied displacement, as the initial delamination grew, it appears that additional delaminations initiate at several other locations. This is indicated by the stress concentrations near the edge of the cutout, and was confirmed with a deformed plot of the sublaminate reference surfaces. Delaminations initiate at both edges of the cutout in the direction parallel to the compressive loads. In addition, a delamination initiates at a distance of approximately 6.0 in. from the edge of the cutout at approximately 135° measured counterclockwise from the 1-direction.

In the experiment for the $d/W = 0.2$ panel, delaminations occur at multiple locations throughout the thickness. The discrepancies of the numerical results with the experimental data are attributed to the fact that the interface elements were not placed between each pair of adjacent laminae of the laminate, but only between one pair of adjacent laminae. However, it is demonstrated that rapid growth of delamination and initiation of delaminations in multiple locations surrounding the cutout can result in catastrophic failure of the panel.

Concluding Remarks

In this paper, results from a PFA that included both intralaminar and interlaminar failures under a geometrically nonlinear response of composite panels containing centrally located circular cutouts are discussed. The PFA was incorporated into a commercial finite element package by developing user-defined subroutines. For intralaminar failure Hashin's criteria was used to predict matrix-cracking mode, fiber-matrix shear mode, and fiber failure mode. Subsequent material degradation is modeled using damage parameters for each mode to selectively reduce lamina material properties. The interlaminar failure modeling was done through interface finite elements. Interface elements were located between sublaminates in the panel near the cutout. A nonlinear constitutive law is postulated for the interface element that accounts for a multi-axial stress criteria to detect the initiation of delamination, a mixed-mode fracture criteria for delamination progression, and a damage parameter to prevent restoration of a previous cohesive state. The PFA was used to model experiments conducted on a flat panel subjected to in-plane shear and curved panel subjected to axial compression.

For both the shear panel and the compression panels, the proposed PFA predicted that intralaminar damage induces the initiation of delamination at the free edge of the cutout at the same locations identified in the experiments. Delamination growth occurred perpendicular to the loading direction in regions where large compressive loads are present. As the shear panel collapsed, a rapid progression of delamination perpendicular to the loading axis was predicted, while delamination arrest was predicted parallel to the loading axis. Delamination growth occurred perpendicular to the compressive loads for the two curved panels with different cutout sizes. The compression panel with smaller diameter cutout-to-width ratio failed with rapid progression of delamination from the edge of the cutout. For the compression panel with larger diameter cutout-to-width ratio, delamination growth was followed by delamination arrest. At this point, the response indicates a residual strength, a finding consistent with the experimental data. After further loading, delamination growth occurs leading to catastrophic failure.

The analyses demonstrated that both intralaminar and interlaminar failure mechanisms were required in the progressive failure methodology to achieve good correlation with the experimental results. Rapid progression of delamination from the edge of the cutout at a location perpendicular to the loading axis was identified as the major cause for catastrophic failure of the panels. Non-self-similar delamination growth, delamination arrest, and closure of delaminated faces were demonstrated throughout the numerical examples.

Acknowledgments

This research is sponsored by the Mechanics and Durability Branch, NASA Langley Research Center, Research Cooperative Agreement NCC-1-398. The authors gratefully acknowledge the technical discussions with Dr. Carlos Dávila from the Analytical and Computational Methods Branch, NASA Langley Research Center, and Prof. Anthony Waas from the Department of Aerospace Engineering of the University Michigan, Ann Harbor.

References

[1]Wang, S., "Fracture Mechanics for Delamination Problems in Composite Laminates," *Journal of Composite Materials, 16*, 1983, pp. 386–394.

[2]Wang, A., "Fracture Analysis of Interlaminar Cracking," *Interlaminar Response of Composite Materials, Composite Material Series, 5. Ed. by N.J. Pagano, Elsevier Science Publishers. Amsterdam, Oxford.*, 1989, pp. 69–109.

[3]Shahwan, K. W. and Waas, A. M., "Non-self similar decohesion along a finite interface of unilaterally constrained delaminations," *Proc. R. Soc. Lond. A., 453, Printed in Great Britain*, 1997, pp. 515–550.

[4]de Moura, M., Marques, J., and de Castro, P., "Modeling Compression Failure after Low Velocity Impact On Laminated Composites Using Interface Elements," *Journal of Composite Materials, 31(15)*, 1997, pp. 1462–1479.

[5]Allix, O. and Corigliano, A., "Geometrical and Interfacial Nonlinearities in the Analysis of Delamination in Composites," *International Journal of Solids and Structures, 36*, 1999, pp. 2189–2216.

[6]Daudeville, L., Allix, O., and Ladevèze, P., "Delamination Analysis by Damage Mechanics: Some Applications," *Composite Engineering, 5(1)*, 1995, pp. 17–24.

[7]Geubelle, P. and Baylor, J., "Impact-Induced Delamination of Composites: a 2D Simulation," *Composites Part B, 29B*, 1998, pp. 589–602.

[8]Dávila, C., Camanho, P., and de Moura, M., "Progressive Damage Analyses of Skin/Stringer Debonding," *Proceedings of the American Society for Composites, 16th Technical Conference, (September 9-12, 2001, Blacksburg, VA) Technomic Publishing Co., Inc., Lancaster PA, CD-ROM.*

[9]Rouse, M., "Effect of Cutouts or Low-speed Impact Damage on the Post-buckling Behavior of Composite Plates Loaded in Shear," *Presented at the AIAA/ASME/ASCE/AHS 31th Structures, Structural Dynamics, and Material Conference, Long Beach, California, April 2-4, 1990. AIAA Paper No. 90-0966-CP.*

[10]Hilburger, M., Britt, V., and Nemeth, M., "Buckling Behavior of Compression-Loaded Quasi-isotropic Curved Panels with a Circular Cutout," *International Journal of Solids and Structures, 38*, 2001, pp. 1495–1522.

[11]Pifko, A. and Kushner, A., "Impact Analysis of Composite Aircraft Structures," *Computational Methods for Crashworthiness, Ahmed K. Noor and Huey D. Carden (Compilers), NASA CP-3223*, 1993.

[12]Sleight, D., Knight, N. J., and Wang, J., "Evaluation of a Progressive Failure Methodology for Laminate Composite Structures," *Proceedings of the AIAA/ASME/ASCE/AHS/ASC 38th Structures, Structural Dynamics, and Materials Conference, April 7-10, 1997, AIAA Paper 97-1187*, pp. 2257–2272.

[13]Dávila, C., Ambur, D., and McGowan, D., "Analytical Prediction of Damage Growth in Notched Composite Panels Loaded in Axial Compression," *Proceedings of the AIAA/ASME/ASCE/AHS/ASC 40th Structures, Structural Dynamics, and Materials Conference, April 12-15, 1999, Paper AIAA-99-1435.*

[14]*ABAQUS User's Manual, Vol. 1-3, Version 5.6*, Hibbitt, Karlsson, and Sorensen, Pawtucket, RI, 1995.

[15]Goyal, V., Johnson, E., Dávila, C., and Jaunky, N., "An Irreversible Constitutive Law for Modeling the Delamination Process Using Interface Elements," *Proceedings of the AIAA/ASME/ASCE/AHS/ASC 43rd Structures, Structural Dynamics, and Materials Conference, April 22-25, 2002, Paper AIAA-2002-1576, CD-ROM.*

[16]Hasin, Z., "Failure Criteria for Unidirectional Fiber Composites," *Journal of Applied Mechanics, 47*, 1980, pp. 329–334.

[17]Chang, F.-K. and Lessard, L., "Damage Tolerance of Laminated Composites Containing an Open Hole and Subjected to Compressive Loadings: Part I- Analysis," *Journal of Composite Materials, 25*, 1991, pp. 2–43.

[18]Ambur, D., Jaunky, N., Dávila, C., and Hilburger, M., "Progressive Failure Studies of Composite Panels with and without Cutouts," *Proceedings of the AIAA/ASME/ASCE/AHS/ASC 42nd Structures, Structural Dynamics, and Materials Conference, April 16-19, 2001, Seattle, Washington, Paper AIAA-2001-1182-CP.*

[19]Jaunky, N., Ambur, D., Dávila, C., and Hilburger, M., "Progressive Failure Studies of Composite Panels with and without Cutouts," *NASA/CR-2001-211223, ICASE Report No. 2001-27*, 2001.

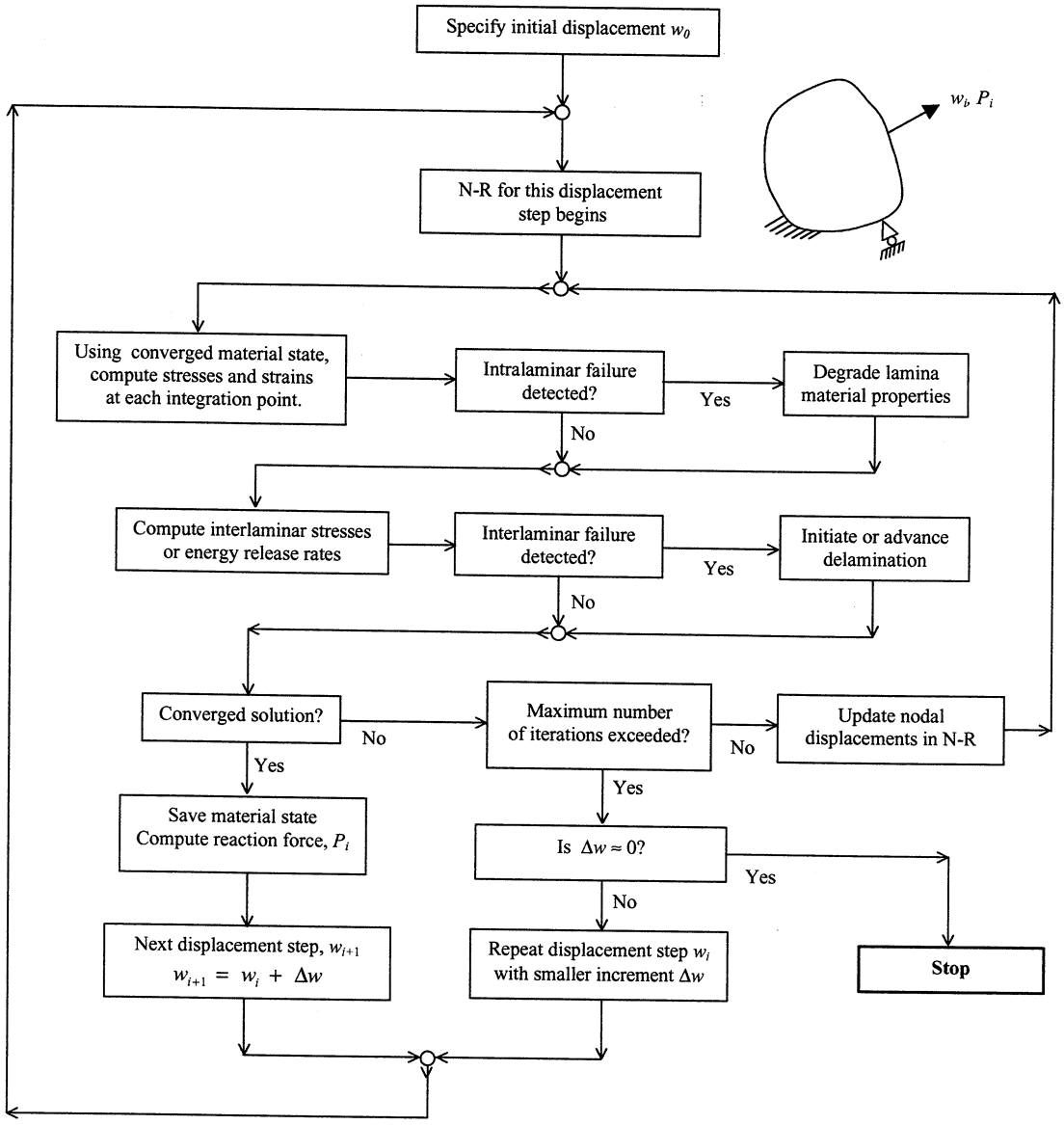

Fig. 1 Typical progressive failure analysis using Newton-Raphson (N-R) for the i-th displacement step.

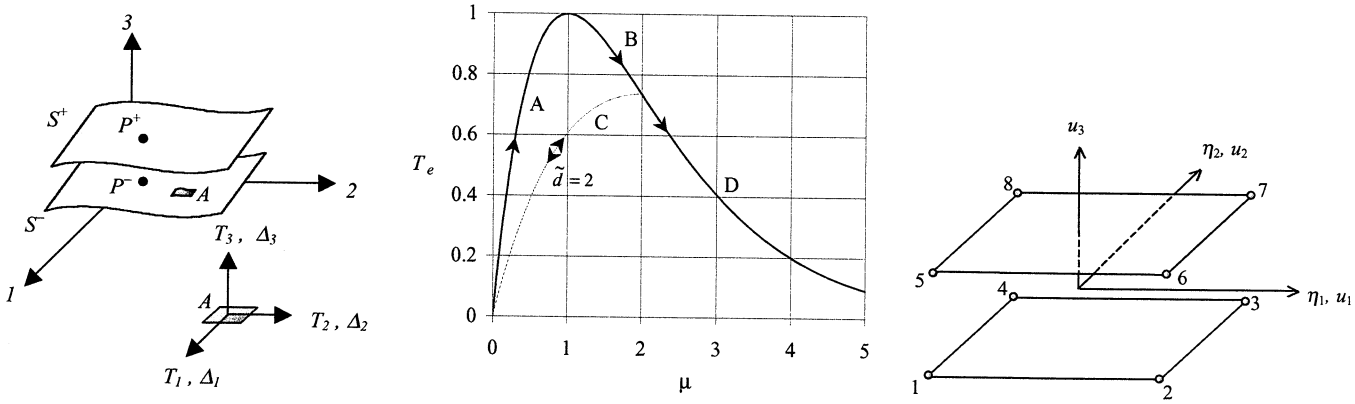

a) Upper and lower surface of an interface material

b) Softening constitutive law

c) Eight node isoparametric interface element

Fig. 2 Features of the interface element.

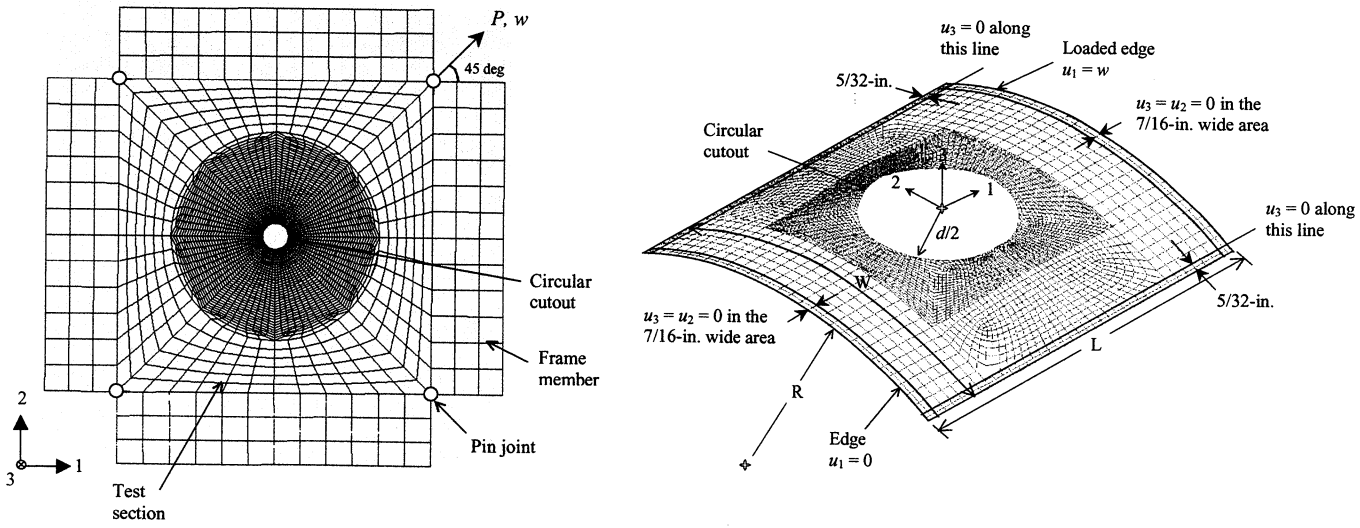

a) Flat panel loaded in shear

b) Curved panel loaded in compression

Fig. 3 Finite element models of the flat and curved composite panels with a centrally located cutout.

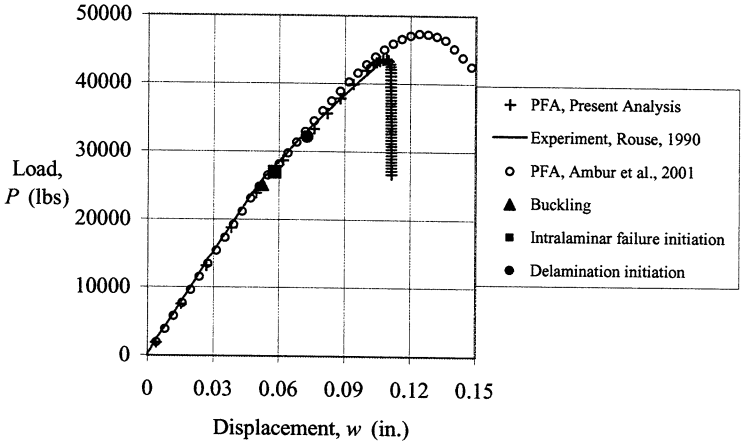

a) Load versus displacement response

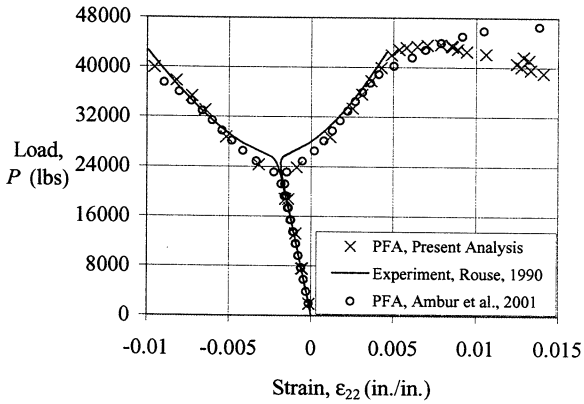

b) Load versus strain component normal to the fiber direction, ε_{22}, in the top and bottom surfaces of the panel

Fig. 4 Response of the flat panel with a cutout and loaded in shear.

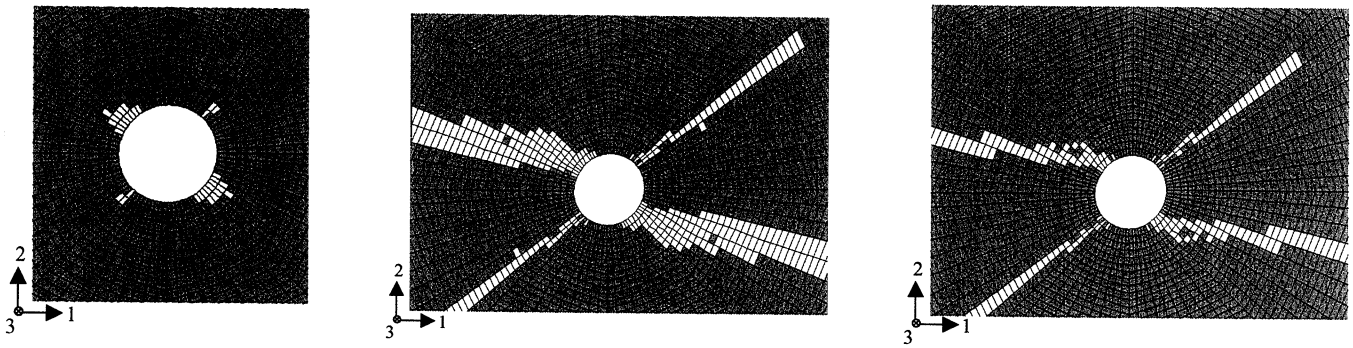

a) Fringe plot of matrix cracking after initiation of damage at $(w, P) = (0.0590, 28.2)$

b) Fringe plot of matrix cracking after progression of damage at $(w, P) = (0.111, 37.6)$

c) Fringe plot of fiber-matrix shear failure after progression of damage at $(w, P) = (0.111, 37.6)$

Fig. 5 Fringe plots of intralaminar damage at the mid-surface of the flat panel.

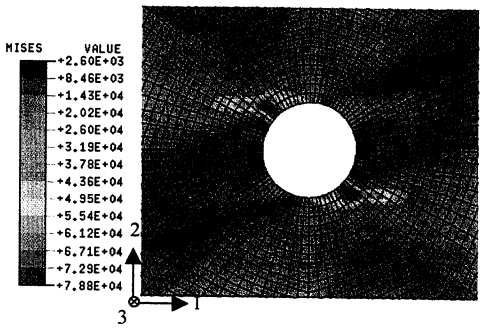

a) Contour plot of the von Mises stresses (psi) at initiation of delamination perpendicular to the load axis, $(w, P) = (0.073, 32.2)$

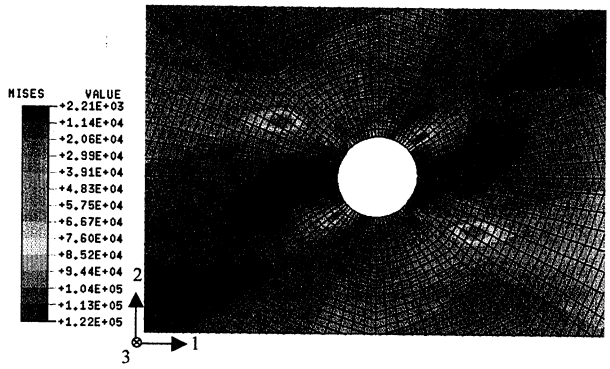

b) Contour plot of the von Mises stresses (psi) at initiation of delamination parallel to the load axis, $(w, P) = (0.107, 43.5)$

Fig. 6 Contour plots of the von Mises stresses (psi) at the mid-surface of the flat panel at two different load levels.

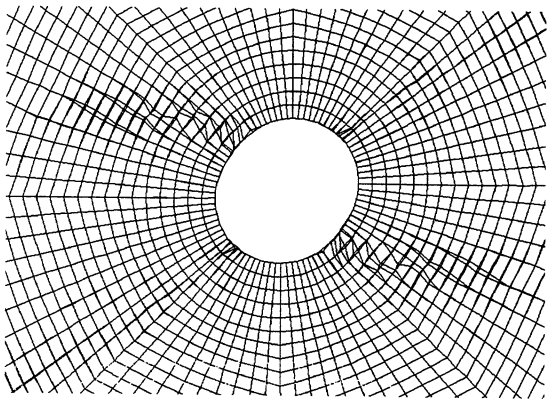

a) Deformed plot of the top and bottom laminates at $(w, P) = (0.107, 43.5)$

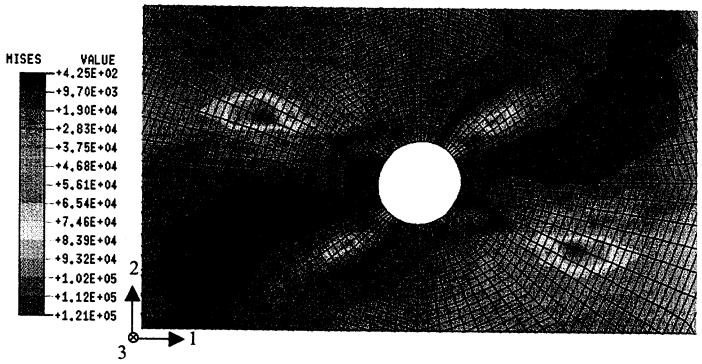

b) Contour plot of the von Mises stresses (psi) after progression of delamination at $(w, P) = (0.111, 40.0)$

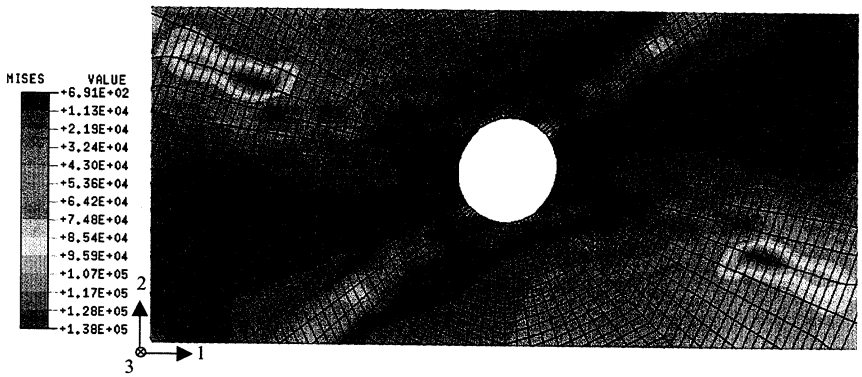

c) Contour plot of the von Mises stresses (psi) after progression of delamination at $(w, P) = (0.112, 30.8)$. Note the reduction in the stress level(psi) parallel to the loading axis

Fig. 7 Deformed plot and contour plots of the von Mises stresses (psi) at the mid-surface of the flat panel corresponding to delamination progression.

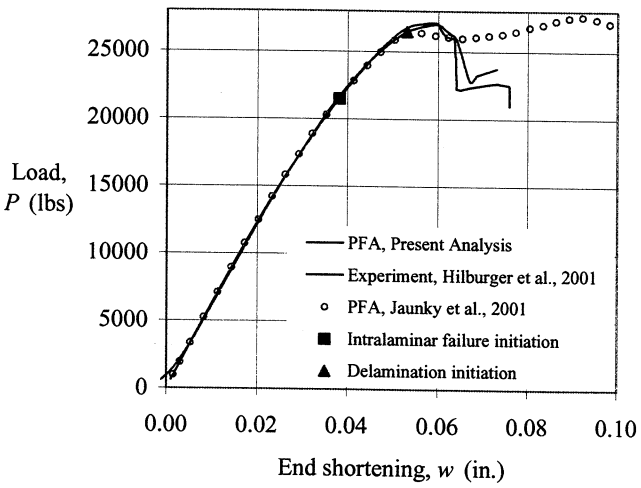

a) $d/W = 0.4$

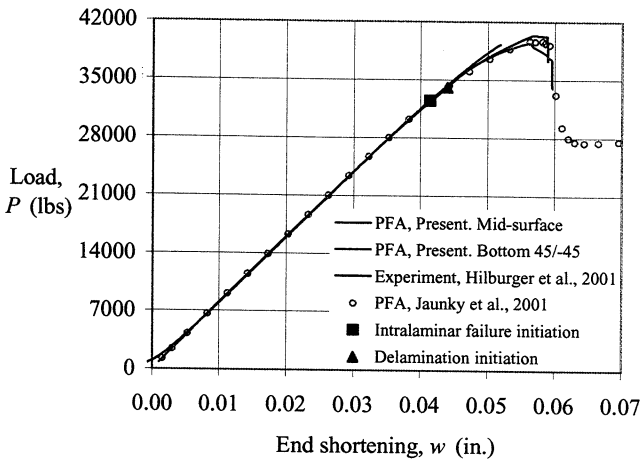

b) $d/W = 0.2$

Fig. 8 Load end-shortening response of the curved panels with a circular cutout and loaded in compression.

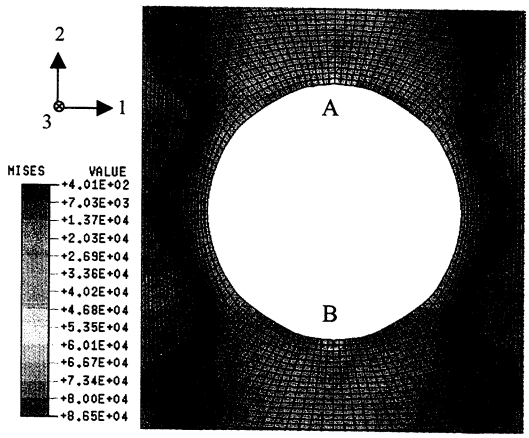

a) Contour plot of the von Mises stresses (psi) at initiation of delamination perpendicular to loading axis

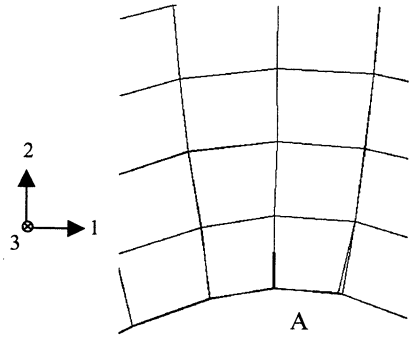

b) Deformed plot of the top and bottom reference surface of the sublaminates

Fig. 9 Contour plot von Mises stresses and deformed plot of reference surfaces at initiation of delamination for curved panel with $d/W = 0.4$ **at** $(w, P) = (0.0530, 26.5)$**.**

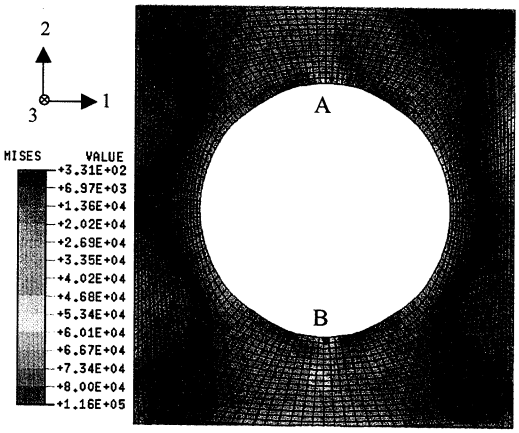

a) Contour plot of the von Mises stresses (psi) after progression of delamination perpendicular to the loading axis

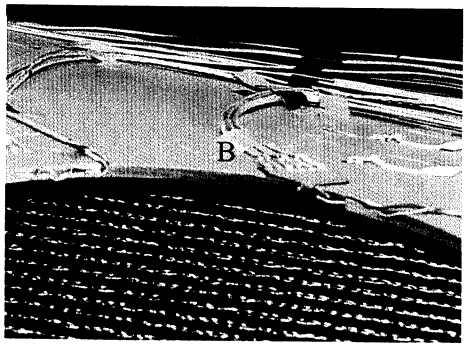

b) Failed test specimen

Fig. 10 Contour plot of von Mises stresses at $(w, P) = (0.0641, 24.7)$ **and failed test specimen of curved panel with** $d/W = 0.4$**.**

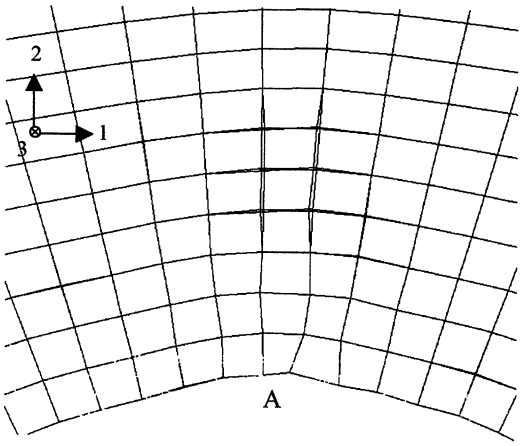

a) Deformed plot illustrates the delaminated region and delamination closure at the top edge near the cutout

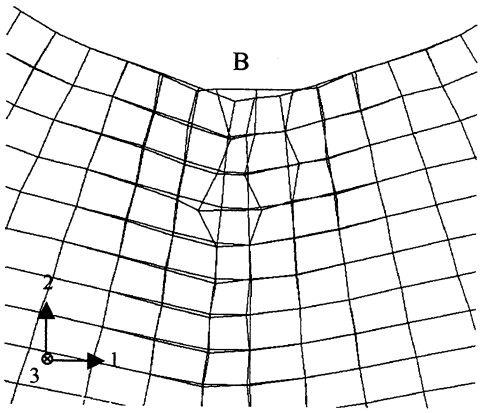

b) Deformed plot illustrates delaminated region at the bottom edge near the cutout

Fig. 11 Deformed plot sublaminate reference surfaces after delamination progresses perpendicular to the loading axis of curved panel with $d/W = 0.4$ at $(w, P) = (0.0641, 24.7)$.

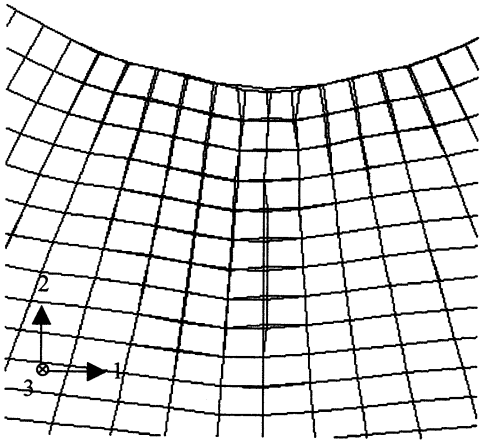

a) Deformed plot of the sublaminate reference surfaces at the bottom edge of the cutout that corresponds to delamination arrest at $(w, P) = (0.071, 22.6)$

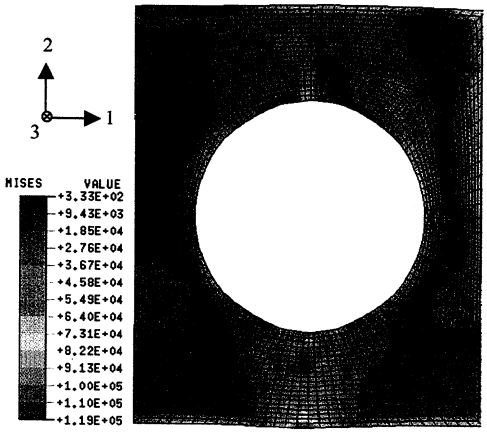

b) Contour plot of the von Mises stresses at failure of the panel, $(w, P) = (0.076, 22.2)$

Fig. 12 Deformed plot and contour plot of the von Mises stresses (psi) at loads corresponding to delamination arrest and failure of curved panel with $d/W = 0.4$.

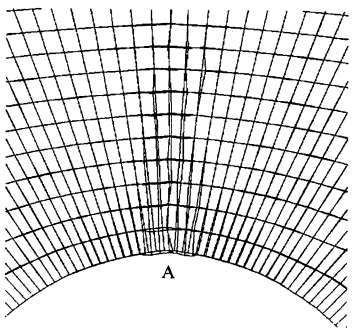

a) Deformed plot of the sublaminate reference surfaces at the top edge of the cutout

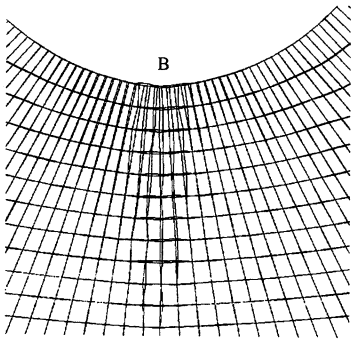

b) Deformed plot of the sublaminate reference surfaces at the bottom edge of the cutout

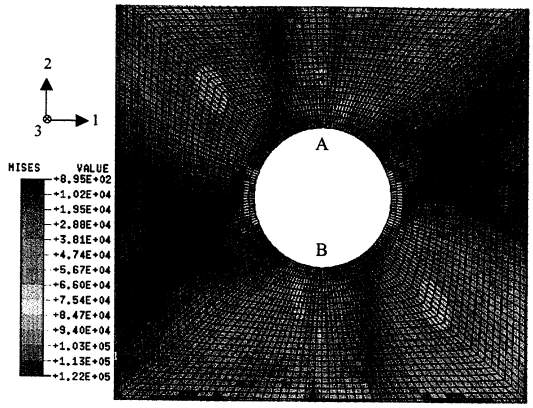

c) Contour plot of the von Mises stresses after progression of delamination

Fig. 13 Deformed plot and contour plot of the von Mises stresses (psi) for initiation and progression of delamination for curved panel with $d/W = 0.2$ at $(w, P) = (0.0595, 35.7)$.